

# CAMEL-CLIP: Channel-aware Multimodal Electroencephalography-text Alignment for Generalizable Brain Foundation Models

Hanseul Choi<sup>a</sup>, Jinyeong Park<sup>a</sup>, Seongwon Jin<sup>a</sup>, Sungho Park<sup>b,\*</sup>,  
Jibum Kim<sup>a,c,\*</sup>

<sup>a</sup>*Department of Computer Science and Engineering, Incheon National University, Yeonsu-gu, 22012, Incheon, Republic of Korea*

<sup>b</sup>*Department of Artificial Intelligence, Inha University, Michuhol-gu, 22212, Incheon, Republic of Korea*

<sup>c</sup>*Center for Brain-Machine Interface, Incheon National University, Yeonsu-gu, 22012, Incheon, Republic of Korea*

---

## Abstract

Electroencephalography (EEG) foundation models have shown promise for learning generalizable representations, yet they remain sensitive to channel heterogeneity, such as changes in channel composition or ordering. We propose channel-aware multimodal EEG-text alignment contrastive language-image pretraining (CAMEL-CLIP), a contrastive EEG-text multimodal foundation model designed to be robust to heterogeneous channel configurations and widely applicable to diverse downstream tasks. CAMEL-CLIP introduces three key components: (1) channel attribute-based positional encoding, which identifies channels through semantic information; (2) dynamic channel projection, which generates variable-length embeddings by independently projecting each channel without feature compression; and (3) dual-level contrastive learning, which jointly performs channel-level and sample-level contrastive learning to capture both channel-specific and global signal characteristics. Experimental results demonstrate that CAMEL-CLIP achieves state-of-the-

---

\*Corresponding to: Department of Computer Science and Engineering, Incheon National University, Yeonsu-gu, 22012, Incheon, Republic of Korea

*Email addresses:* himlm0704@gmail.com (Hanseul Choi), devslem12@gmail.com (Jinyeong Park), jinwork00@gmail.com (Seongwon Jin), sungho.park@inha.ac.kr (Sungho Park), jibumkim@inu.ac.kr (Jibum Kim)

art performance under linear-probing and outperforms existing foundation models that rely on full-finetuning.

*Keywords:* Brain-computer interface, Electroencephalography, Multimodal learning, Foundation model, Contrastive learning, Channel heterogeneity

---

## 1. Introduction

Electroencephalography (EEG) is widely used across clinical applications and brain-computer interface (BCI) research, with applications including seizure detection, depression monitoring, Alzheimer’s disease diagnosis, motor imagery, and image reconstruction. To decode EEG signals, numerous deep learning models have been proposed (Ay et al., 2019; Shoeibi et al., 2021; Solis-Escalante et al., 2024). These approaches can be broadly categorized into several paradigms based on their methodological characteristics.

As a first paradigm in deep learning-based EEG decoding, task-specific models such as EEGNet (Lawhern et al., 2018), EEG Conformer (Song et al., 2023), and CNN-LSTM feature fusion network (FFCL) (Li et al., 2022) have been proposed. These models are lightweight in terms of model parameter size and can effectively process EEG signals. However, since only a limited number of subjects are typically available for each task, they have difficulty in exploiting large-scale datasets. Consequently, they are vulnerable to domain shifts such as inter-subject variability and often exhibit poor generalization performance (Saha and Baumert, 2020).

As a new paradigm to overcome the limited generalization of these task-specific models, self-supervised brain foundation models such as Large Brain Model (LaBraM) (Jiang et al., 2024) and a criss-cross brain foundation model for EEG decoding (CBraMoD) (Wang et al., 2024) have been proposed. By using large-scale datasets, these models are able to learn general-purpose representations and significantly outperform earlier approaches, while showing relatively strong robustness to inter-subject variability. However, they remain sensitive to cross-dataset domain shifts, such as differences in recording settings and changes in channel configurations, and can suffer substantial performance degradation without an additional finetuning step (Xiong et al., 2025).

Existing models typically learn inter-channel dependencies tied to the channel ordering defined in the training dataset. Consequently, when a domain shift involves changes in channel composition or ordering, the model often

fails to adapt effectively (Zhang et al., 2025). The model cannot effectively reuse its learned knowledge when extracting features under a new channel configuration. This makes it difficult to use pretrained models via linear-probing (Kuruppu et al., 2025). This problem is referred to as cross-dataset channel heterogeneity. Chen et al. (2025) proposed an EEG foundation model that leverages the spatial coordinates of electrodes to address this issue. However, this coordinate-based approach still has limitations, as it cannot capture other factors such as reference type (Yao et al., 2019), which can substantially affect signal characteristics.

The majority of existing brain foundation models are trained using a single modality, making the results suffer from low explainability. The limited explainability of these models mainly stems from a lack of semantic alignment between EEG data and human-understandable modalities like natural language. To overcome the limitations of unimodal learning, Ndir et al. (2025) proposed the first contrastive language-image pretraining (CLIP)-based multimodal model, named EEG-CLIP. For effective EEG-text alignment, they employed the TUAB dataset, an EEG-text paired dataset. They demonstrated that text-based classification can be performed without an additional classifier. It also highlights the potential of using contrastive learning for EEG-text multimodal models. However, due to its poor generalization performance regarding channel heterogeneity and overfitting to the training dataset, EEG-CLIP is difficult to utilize as a pretrained model.

We propose the first contrastive EEG-text multimodal foundation model, namely channel-aware multimodal EEG-text alignment contrastive language-image pretraining (CAMEL-CLIP) designed to be invariant to varying channel configurations. First, to mitigate channel heterogeneity, we introduce a novel channel positional encoding method called channel attribute-based positional encoding. Inspired by the EEG electrode naming convention, we generate channel positional embeddings based on the attributes of each channel. This allows the model to identify each channel even if the channel positions change within a data sample.

Second, many previous works either assume a fixed number of channels or perform pooling along the channel axis, thereby constraining the model to produce only fixed-length embeddings. To address this limitation, we propose dynamic channel projection, which applies channel-wise independent projection layers and integrates textual reports with channel information to generate variable-length embeddings. Specifically, this module adjusts the length of the text embeddings to match the dimensionality of the EEG embeddings,



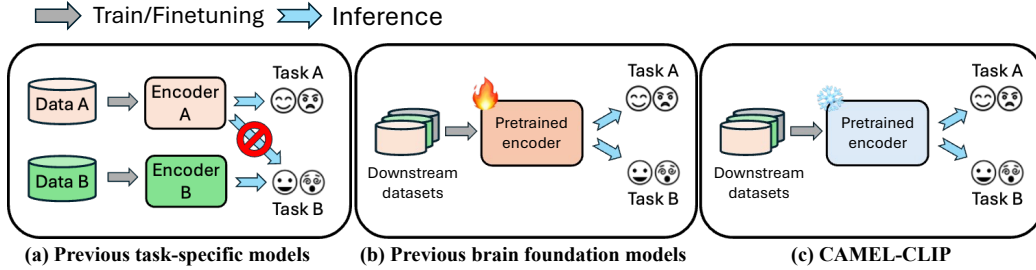


Figure 2: **Paradigm shift in deep learning-based EEG decoding.** (a) Conventional task-specific models, where a separate EEG encoder is trained for each task and dataset. (b) Prior brain foundation models, which enable multi-task transfer via pretrained weights but still require finetuning on downstream datasets due to channel heterogeneity. (c) CAMEL-CLIP, which mitigates channel heterogeneity and supports multiple tasks with linear-probing alone.

which does not exhibit channel-level separation, CAMEL-CLIP learns distinct channel-specific feature distributions that are clearly separable across channels.

Figure 2 compares each paradigm in deep learning-based EEG decoding, highlighting the shift enabled by the proposed approach. Figure 2(a) illustrates the task-specific model paradigm, where a separate encoder must be trained for each dataset (Lawhern et al., 2018; Song et al., 2023). Figure 2(b) shows the full-finetuning paradigm of prior brain foundation models (Jiang et al., 2024; Wang et al., 2024). Figure 2(c) presents the new paradigm, CAMEL-CLIP, where a single pretrained encoder supports multiple tasks via linear-probing alone, without finetuning the encoder.

The main contributions of this paper are summarized as follows:

1. As a new paradigm for EEG decoding, we propose CAMEL-CLIP, an EEG-text multimodal foundation model designed to be resilient to channel variations and broadly applicable to diverse downstream tasks.
2. We effectively mitigate the issue of channel heterogeneity through the introduction of our novel positional encoding and contrastive learning techniques.
3. We demonstrate the clinical utility of CAMEL-CLIP by enabling complex cross-modal tasks, such as EEG-text retrieval.
4. CAMEL-CLIP achieves strong generalization across a wide range of downstream tasks using only linear-probing, consistently outperforming existing state-of-the-art methods.

## 2. Related works

### 2.1. Task-specific EEG decoding models

Lawhern et al. (2018) proposed EEGNet, a lightweight architecture that effectively extracts spatiotemporal EEG features using depthwise separable convolutions. Subsequently, Li et al. (2022) introduced FFCL, which improves classification performance by fusing features extracted from different layers of convolutional neural network (CNN) and long short-term memory (LSTM) backbones. While these task-specific models are practically efficient due to their small parameter footprint, they struggle to learn generalizable representations from large-scale datasets. Furthermore, they remain highly susceptible to inter-subject variability even within small datasets, often necessitating repeated data collection and model retraining for each novel subject or target task.

### 2.2. Brain foundation models

Many previous works have proposed brain foundation models for neural decoding. Yang et al. (2023) developed biosignal transformer (BIOT), which utilizes a standardized tokenization strategy to extract universal features across diverse physiological signals like EEG and ECG. Focusing on architectural refinement, Wang et al. (2024) presented CBraMod. This model leverages a criss-cross attention mechanism to independently process the distinct spatial and temporal dynamics inherent in EEG recordings. Furthermore, Jiang et al. (2024) pushed the boundaries of scale with LaBraM, training on an extensive 2,500-hour corpus. By implementing a Fourier-based neural tokenizer, they established one of the most extensively parameterized models in the field. However, despite these substantial breakthroughs, a critical gap remains: these state-of-the-art frameworks are exclusively unimodal. This singular focus inherently precludes them from executing complex cross-modal operations, such as mapping EEG signals directly to textual clinical reports.

### 2.3. EEG-text multimodal contrastive learning models

Recent studies have explored contrastive learning between EEG signals and textual data. Yan et al. (2025) proposed an EEG-text multimodal contrastive learning model for emotion recognition. By aligning EEG representations to the rich semantic space provided by a text encoder, their method learns domain-invariant representations, and empirical results indicate that multimodal contrastive learning can improve cross-domain generalization. However,

due to the scarcity of informative EEG-text paired data, the approach is largely limited to emotion recognition. Ndir et al. (2025) leveraged EEG recordings and clinical text reports to train a model using CLIP-based contrastive learning (Radford et al., 2021). While this work demonstrated the feasibility of text-based classification in the EEG domain, it reported limited generalization, achieving approximately 0.56 balanced accuracy on a gender classification task. Overall, existing contrastive EEG-text multimodal models are often either task-specific or insufficiently generalizable, limiting their applicability to diverse downstream tasks.

#### 2.4. Channel-Invariant EEG models

To manage channel inconsistencies across datasets, Patil et al. (2024) utilized 3D positional data to capture the spatial dependencies between electrodes. Yet, such coordinate-dependent methods demand precise localization, limiting their utility on legacy datasets missing these anatomical annotations. Similarly, Chen et al. (2025) introduced a foundational architecture relying on static electrode positions extracted from a standardized head template. However, the fundamental constraints of coordinate-centric designs prevent seamless adaptation to bipolar montages. Furthermore, they fail to account for non-spatial variables, such as the choice of reference, which drastically alter signal properties. Shifting away from spatial coordinates, Yi et al. (2023) developed a pretraining framework with multi-dimensional position encoding, multi-level channel hierarchy, multi-stage pretraining strategy (MMM) to project varying channel setups onto a static 62-node graph. Nonetheless, this fixed mapping struggles to accommodate channel arrays that fall outside the assumed structure, and extracting differential entropy features risks discarding critical signal information.

### 3. Methods

#### 3.1. Overall architecture

Figure 3 provides an overview of the proposed model, CAMEL-CLIP. The model has five key components: a text encoder, an EEG encoder, channel attribute-based positional encoding (CAPE), dynamic channel projection (DCP), and dual-level contrastive learning (DCL). Given an EEG-text pair as input, the EEG and text encoders extract modality-specific features. The EEG encoder incorporates CAPE to encode channel location information.

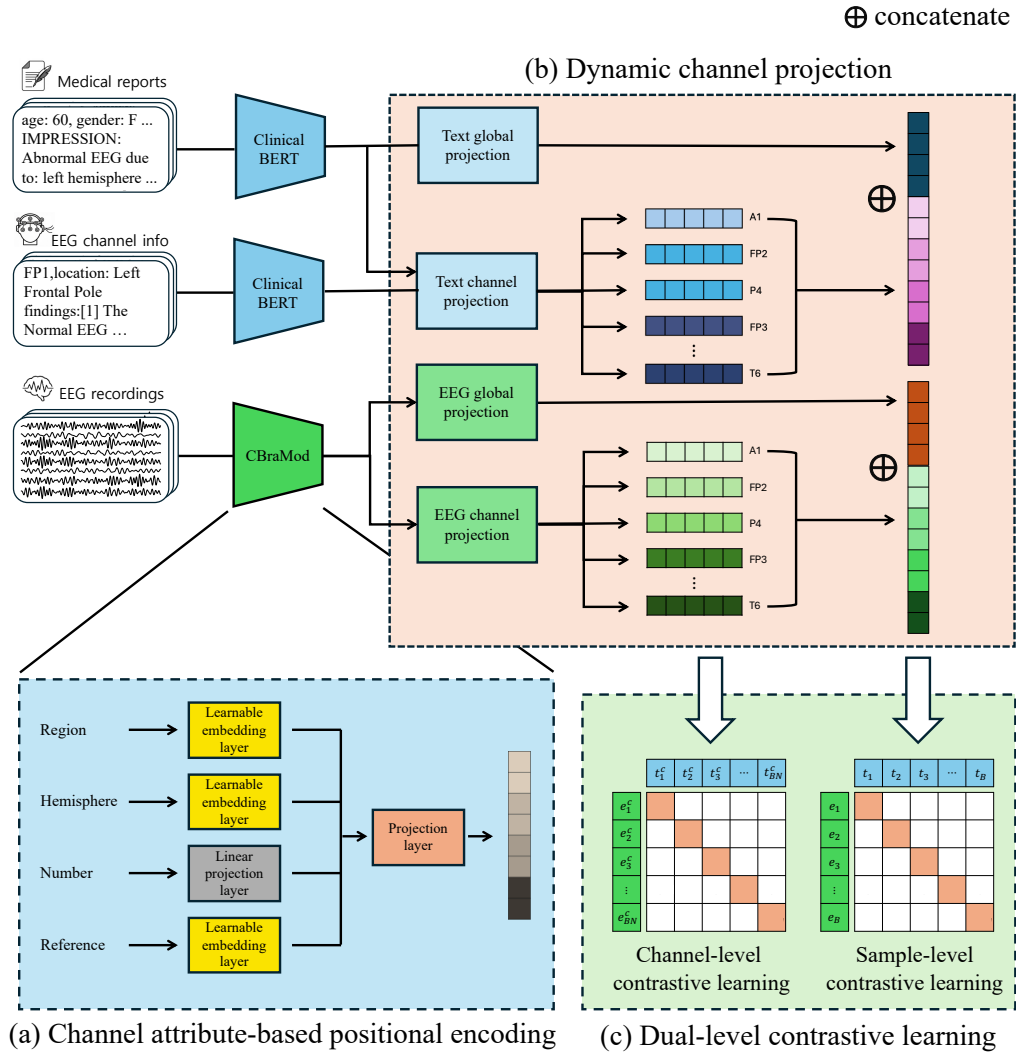


Figure 3: **Framework of the proposed model.** (a) Channel attribute-based positional encoding. (b) Dynamic channel projection for channel-wise embeddings. (c) dual-level contrastive learning at the channel and sample levels. Here, A1, FP2, P4, FP3, and T6 annotate example channel names.

The outputs of both encoders are then mapped to embeddings for contrastive learning via DCP, and the model is trained with the proposed dDCL scheme.

**Text encoder.** We adapt ClinicalBERT (Huang et al., 2019) as the text encoder in our model. ClinicalBERT is a BERT (Devlin et al., 2019) model pretrained on electronic health records (EHRs) and is well aligned with the linguistic characteristics of clinical EEG reports, which differ substantially from general-domain text in both style and context. During contrastive training, we initialize the text encoder with pretrained weights and keep it frozen to mitigate overfitting.

**EEG encoder.** We adapt the self-supervised pretrained model CBraMoD (Wang et al., 2024) as the EEG encoder. CBraMoD is designed to disentangle temporal and spatial characteristics during representation learning. To generate channel positional encodings independent of channel order, we introduce a new CAPE module. Aside from this modification, we initialize the EEG encoder with the pretrained CBraMoD weights and finetune the remaining parameters during training.

### 3.2. Channel attribute-based positional encoding

To alleviate the performance drop induced by channel heterogeneity (Xiong et al., 2025), we introduce CAPE. Drawing inspiration from established EEG nomenclatures (Jasper, 1958), CAPE categorizes channels using four distinct features: (1) region (scalp area), (2) hemisphere (lateral position), (3) number (proximity to the midline), and (4) reference type. By leveraging these characteristics, we assign a tailored positional embedding to each channel that captures its spatial and referencing properties (Yao et al., 2019), allowing the architecture to seamlessly discern individual channel identities. For the encoding process, categorical variables (*i.e.*, region, hemisphere, and reference type) are mapped via learnable embedding layers, while the continuous variable (*i.e.*, number) undergoes a linear projection to maintain spatial continuity. These four intermediate representations are subsequently concatenated and fed into a multilayer perceptron, yielding a comprehensive channel embedding that explicitly delineates its spatial configuration.

Bipolar montages inherently capture the potential variance between a pair of electrodes (Yao et al., 2019). To accurately model this dynamic, we define the embedding of a bipolar channel as the mean of its constituent electrode embeddings. This design allows the model to transfer unipolar insights seamlessly into bipolar contexts.

### 3.3. Dynamic channel projection

To preserve the distinct representational properties of individual EEG channels, we propose DCP, a module that formulates and concatenates independent embeddings for each channel. This approach facilitates the extraction of highly granular features. Specifically, channel-specific text embeddings are produced by fusing a patient’s clinical report embedding with a channel knowledge embedding via a fully connected layer. These channel knowledge embeddings are derived by encoding anatomical and medical descriptions sourced from literature using the text encoder. Consequently, this architecture supports contrastive learning across variable channel counts without necessitating the compression of channel-specific data.

Furthermore, DCP inherently supports dynamic channel removal, a stochastic data augmentation strategy applied during training. For any given mini-batch, this technique is triggered with a predefined probability,  $p_{remove}$ . Once activated, a subset of channels—drawn uniformly from the range  $[1, C \cdot r_{max}]$ , where  $C$  is the total channel count and  $r_{max}$  is the maximum removal threshold—is randomly discarded. For example, given a 20-channel setup with  $p_{remove} = 0.3$  and  $r_{max} = 0.5$ , roughly 30% of the training batches will randomly lose between 1 and 10 channels. This strategic perturbation compels the model to adapt to varying channel availability, drastically improving its robustness to channel configuration shifts.

### 3.4. Dual-level contrastive learning

We propose DCL to enable the model to extract meaningful features for unseen channels by leveraging learned representations. This training scheme encourages the EEG encoder to jointly learn channel-specific embeddings that capture distinct channel characteristics and a global embedding that summarizes the overall signal. DCL comprises two contrastive objectives, Channel-Level Contrastive Learning (CCL) and Sample-Level Contrastive Learning (SCL), both based on the InfoNCE objective (van den Oord et al., 2018).

CCL is introduced to learn channel-level representations. In CCL, the channel-wise EEG embedding and the corresponding channel-wise text embedding from the same sample and the same channel are treated as a positive pair. All other channel embeddings from the same sample (*i.e.*, different channels) as well as embeddings from other samples are treated as negative pairs. For training efficiency, we randomly sample  $N$  channels from each sample in a

mini-batch and apply contrastive learning at the channel-embedding level. The CCL loss is defined as follows:

$$L_{CCL} = -\frac{1}{2BN} \sum_{i=1}^{BN} \left( \log \frac{\exp(e_i^{c\top} t_i^c / \tau)}{\sum_{j=1}^{BN} \exp(e_i^{c\top} t_j^c / \tau)} + \log \frac{\exp(t_i^{c\top} e_i^c / \tau)}{\sum_{j=1}^{BN} \exp(t_i^{c\top} e_j^c / \tau)} \right), \quad (1)$$

where  $e_i^c$  denotes the  $i$ -th channel-wise EEG embedding and  $t_i^c$  denotes the  $i$ -th channel-wise text embedding.  $B$  is the batch size,  $N$  is the number of sampled channels per sample, and  $\tau$  is the temperature parameter.

SCL constructs a sample-level global embedding by applying attention pooling over the channel embeddings and their corresponding channel features. Contrastive learning is then applied to the concatenated representation of the global embedding and the channel embeddings. This global embedding is motivated by the fact that CCL emphasizes channel-specific representations, which can make it harder for individual channel embeddings to capture patterns shared across channels. To encourage learning of such channel-invariant characteristics, the global EEG embedding is aligned with a text embedding obtained by projecting only the clinical report embedding, without incorporating channel information. The SCL loss is defined as follows:

$$L_{SCL} = -\frac{1}{2B} \sum_{i=1}^B \left( \log \frac{\exp(e_i^\top t_i / \tau)}{\sum_{j=1}^B \exp(e_i^\top t_j / \tau)} + \log \frac{\exp(t_i^\top e_i / \tau)}{\sum_{j=1}^B \exp(t_i^\top e_j / \tau)} \right), \quad (2)$$

Here,  $e_i$  denotes the  $i$ -th EEG embedding,  $t_i$  denotes the  $i$ -th text embedding,  $B$  is the batch size, and  $\tau$  is the temperature parameter.

To prevent the model from being overly dominated by the CCL loss such that the intended SCL objective is not effectively optimized, we weight CCL by a factor of  $\lambda$  when combining the losses. The overall objective is defined as follows:

$$L_{DCL} = L_{SCL} + \lambda \cdot L_{CCL}. \quad (3)$$

### 3.5. Synthetic Report Ensemble Prompt Generation

Text embeddings derived from conventional single-sentence prompts often exhibit a significant distributional shift from the representations inherently learned by the model. Consequently, these simplistic prompts fail to accurately capture the true semantic space of each label. To resolve this discrepancy, we introduce a novel technique termed synthetic report ensemble prompt

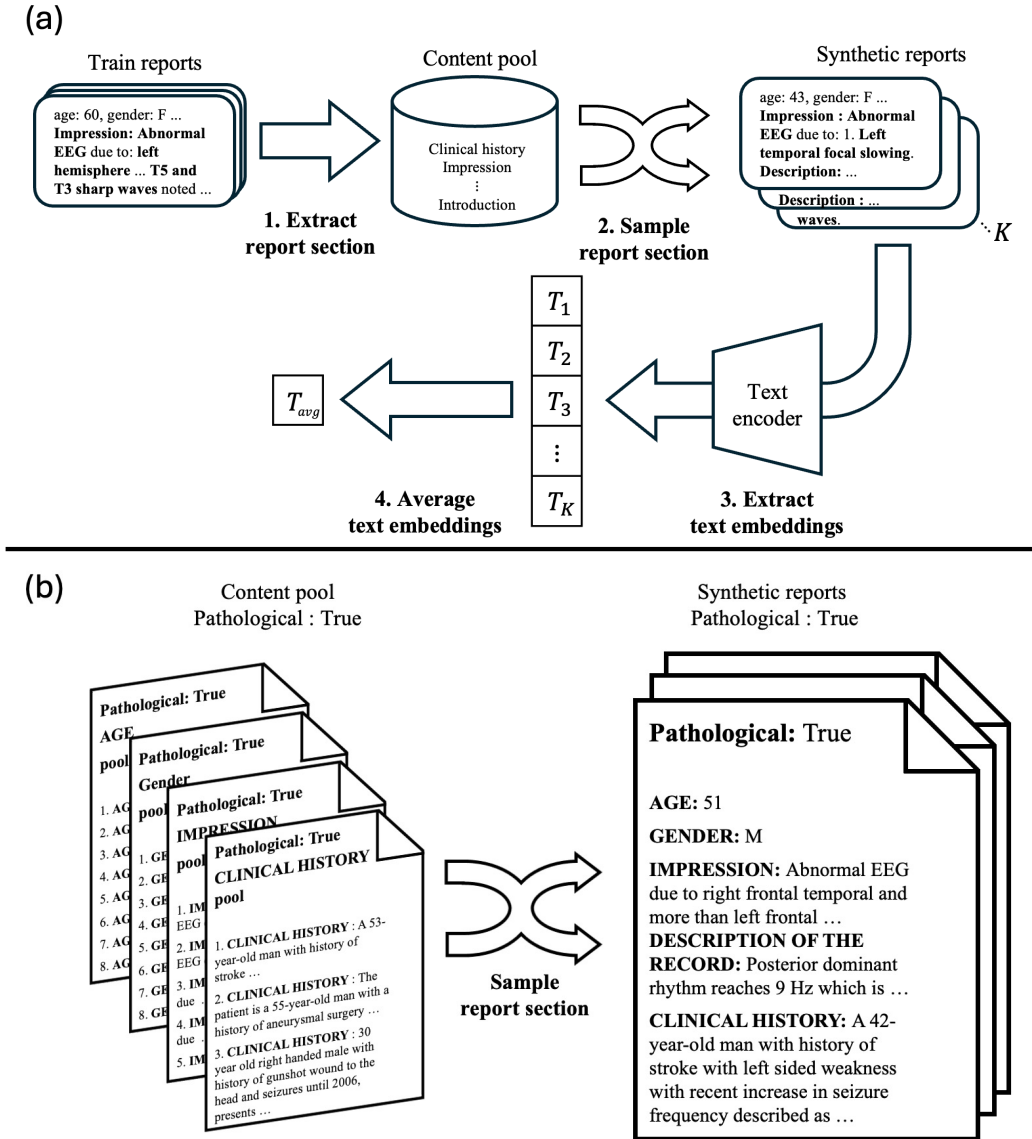


Figure 4: **Pipeline of proposed synthetic report ensemble prompt generation.** (a) The proposed text prompt generation method for text-based classification generates multiple synthetic reports and averages their embeddings. (b) An example of generated synthetic report.

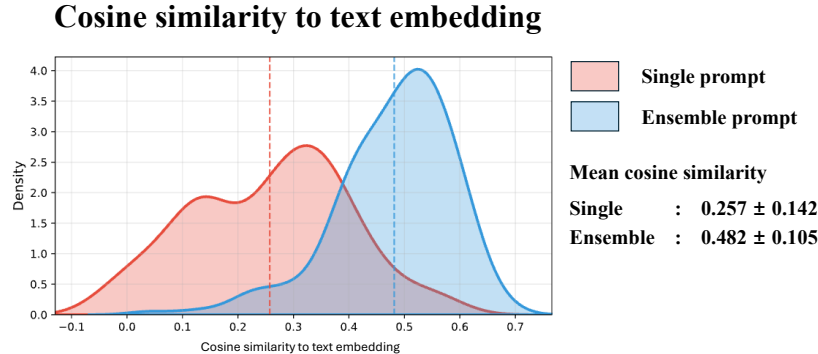


Figure 5: **Cosine similarity distributions across prompting strategies.** Cosine similarity between prompts for normal labels in the pathological task and text embeddings from the validation set. The prompts from the proposed ensemble method show a higher mean cosine similarity.

generation. This approach first dissects training reports into discrete structural sections, aggregating them by class to form label-specific content pools. During inference, we synthesize  $K$  distinct reports by uniformly sampling and concatenating one text segment from each section’s pool. The final text prototype for a given label is then computed as the average embedding of these  $K$  synthetic reports. For instance, in a binary pathology classification task (*normal* vs. *abnormal*), the *normal* prototype is formulated by independently drawing segments from pools such as clinical history, medications, and impression—all exclusively sourced from normal cases. After generating  $K$  such reports, their embeddings are averaged to establish the robust *normal* prototype.

Figure 4 (a) illustrates the proposed framework for generating averaged report embeddings. Figure 4 (b) shows an example of generated synthetic report. The label embedding for label  $y$  is computed by averaging the text-encoder embeddings of  $K$  synthetic reports:

$$E_y = \frac{1}{K} \sum_{k=1}^K \text{Textencoder}(T_{\text{synthetic},y}^k), \quad (4)$$

where  $K$  is the number of synthetic reports and  $T_{\text{synthetic},y}^k$  denotes the  $k$ -th synthetic report for label  $y$ .

To demonstrate the efficacy of our averaged report embedding strategy, we evaluated the cosine similarity distributions on the TUAB dataset (Obeid

and Picone, 2016). Specifically, we measured the alignment between the text prototypes generated for the *normal* pathology label and the actual distribution of clinical reports in the validation set. As illustrated in Figure 5, the embeddings derived via our proposed ensemble approach exhibit a substantially higher mean cosine similarity than the single-prompt baseline. Quantitatively, the single-prompt method yields a mean similarity of 0.257, whereas our proposed technique achieves 0.482. These findings confirm that the synthetic report ensemble prompt generation method captures the semantic distribution of the target labels far more accurately than conventional single-sentence prompts.

## 4. Experimental settings

### 4.1. Datasets

**TUAB dataset.** This dataset is a subset of the Temple University Hospital EEG Data Corpus (Obeid and Picone, 2016) and labels each patient as normal or abnormal. The recordings use an average reference montage with 21 channels. The TUAB dataset includes 1,237 normal and 893 abnormal subjects in the training split, and 148 normal and 105 abnormal subjects in the evaluation split. Each patient report consists of 15 fields, including metadata such as *age* and *gender*, as well as clinical symptoms and examination findings. In this work, we use the report content to perform binary classification on three labels: *pathological*, *gender*, and *age*. For the age label, we classify patients into two groups, those aged 50 years or older and those younger than 50 years.

**CHB-MIT dataset.** This dataset contains EEG recordings from 22 pediatric patients with intractable seizures (Shoeb, 2009; Goldberger et al., 2000; Guttag, 2010). The recordings use a bipolar montage with 23 channels. Patients 1 to 19 are used for training, patients 20 and 21 for validation, and patients 22 and 23 for evaluation.

**MUMTAZ-2016 dataset.** This dataset was collected from 34 patients with major depressive disorder and 30 healthy controls (Mumtaz, 2016). The recordings use a linked ear reference montage with 19 channels. The training split includes 24 patients with major depressive disorder and 19 controls, the validation split includes 5 patients and 4 controls, and the evaluation split includes 5 patients and 5 controls.

Table 1: **Average text-based classification balanced accuracy across varying dynamic channel removal probability  $p_{remove}$ .** This table reports the mean balanced accuracy of text-based classification on the TUAB validation set for different removal probabilities.

$p_{remove}$	Balanced accuracy
0	0.7330
0.25	0.7325
0.50	<b>0.7442</b>
0.75	0.7230

Table 2: **Average text-based classification balanced accuracy across CCL sampling values of  $n$ .** This table reports the mean balanced accuracy of text-based classification on the TUAB validation set for different CCL sampling values of  $n$ .

n	Balanced accuracy
1	0.7387
<b>3</b>	<b>0.7442</b>
5	0.7416

#### 4.2. Implementation details

We trained the proposed model for 100 epochs with a mini-batch size of 512. Without early stopping, we evaluated text-based classification on the validation set at every epoch for three tasks (*i.e.*, pathological, gender, and age) and selected the checkpoint with the highest mean balanced accuracy across tasks. Both the global and channel embedding dimensions were set to 64. Dynamic channel removal was applied with  $p_{remove} = 0.5$ ,  $r_{max} = 0.8$ . The  $p_{remove}$  was chosen via the hyperparameter search in Table 1. For CCL, we set the channel sampling number  $n$  to 3 based on the hyperparameter search in Table 2. We set  $\lambda$  to 0.5. For evaluation with a classifier, each model was trained five times with five different random seeds.

## 5. Experiments

In this section, we conduct a diverse set of experiments to evaluate the effectiveness of CAMEL-CLIP. Table 3 summarizes the objectives and procedures of the experiments in this work.

**Experiment 1** performs text-based classification to assess whether the proposed contrastive training (DCL) achieves effective EEG-text alignment.

Table 3: **Summary of experiments.** This table summarizes the objective and procedure of each experiment.

Experiment	Experiments type	Dataset	Goal
Experiment 1	Text-based classification	TUAB	Evaluate EEG-text alignment quality through text-based classification with single/ensembled prompt
Experiment 2	Channel representation analysis	TUAB	Validate the effectiveness of channel-level contrastive learning
		CHB-MIT	
Experiment 3	Classification with classifier	TUAB	Evaluate model performance on various datasets
		CHB-MIT	
		MUMTAZ-2016	
Experiment 4	Text-based classification	TUAB	Ablation study
	Classification with classifier	CHB-MIT	
		MUMTAZ-2016	
Experiment 5	Retrieval	TUAB	Evaluate model performance on EEG-text retrieval task

**Experiment 2** evaluates the impact of the proposed CCL by visualizing and analyzing the channel-wise embedding distributions and their similarities. **Experiment 3** investigates whether the EEG encoder learned by the proposed framework extracts generalizable features across datasets. We attach an additional classifier, finetune the model, and report performance under both full-finetuning and linear-probing settings on downstream datasets. **Experiment 4** conducts an ablation study to validate the contribution of each component of the proposed method to overall performance. **Experiment 5** measures EEG-text retrieval performance to assess the potential utility of the proposed model in clinical diagnostic settings.

When using TUAB datasets, we set the baseline model as the EEG-CLIP (Ndir et al., 2025). This is because the TUAB dataset is a multimodal EEG-text dataset and the only existing EEG-text multimodal model based on the TUAB dataset is the EEG-CLIP model.

Table 4: **Text-based classification (single prompt)**. This table reports text-based classification performance on the three TUAB tasks using a single prompt.

Methods	<i>pathological</i>	<i>gender</i>	<i>age</i>
EEG-CLIP	0.4467	0.5360	0.4395
<b>Proposed</b>	<b>0.5640</b>	<b>0.6437</b>	<b>0.6751</b>

Table 5: **Text-based classification (ensemble prompt)**. This table reports text-based classification performance on the three TUAB tasks using ensemble prompts.

Methods	<i>pathological</i>	<i>gender</i>	<i>age</i>
EEG-CLIP	0.7905	0.5608	0.6718
<b>Proposed</b>	<b>0.8158</b>	<b>0.6463</b>	<b>0.7125</b>

### 5.1. EEG-text alignment evaluation

In Experiment 1, we assess the cross-modal alignment capabilities of our model. By employing cosine similarity to match EEG embeddings against class-specific text prompts, we directly evaluate the quality of the learned representations. Because the EEG-CLIP baseline inherently utilizes a single-prompt classification scheme, we conduct our evaluations under both single-prompt and the proposed ensemble-prompt (*i.e.*, synthetic report ensemble prompt) settings to maintain fair comparative conditions.

Table 4 demonstrates that CAMEL-CLIP uniformly outperforms the baseline across all three tasks in the single-prompt scenario, achieving notable margins of up to 23.6%. This trend is corroborated in table 5, where the models are tested using synthetic report ensemble prompts; here, CAMEL-CLIP again exceeds baseline performance by up to 8.5%. Overall, these empirical results validate that the proposed CAMEL-CLIP architecture significantly enhances EEG-text embedding alignment.

### 5.2. Effectiveness of channel-level contrastive learning

Experiment 2 investigates the impact of CCL through a detailed analysis of embedding distributions. First, UMAP visualizations (McInnes et al., 2018) confirm that the CCL objective forces the encoder to extract highly individualized channel embeddings. Figure 6 reveals that the CCL-trained model forms tightly separated clusters, unlike the non-CCL baseline, proving its ability to capture channel-specific semantics.

Next, we examine zero-shot generalization by removing five channels (F4, FZ, O1, P3, and T3) during training in the TUAB dataset. Comparing

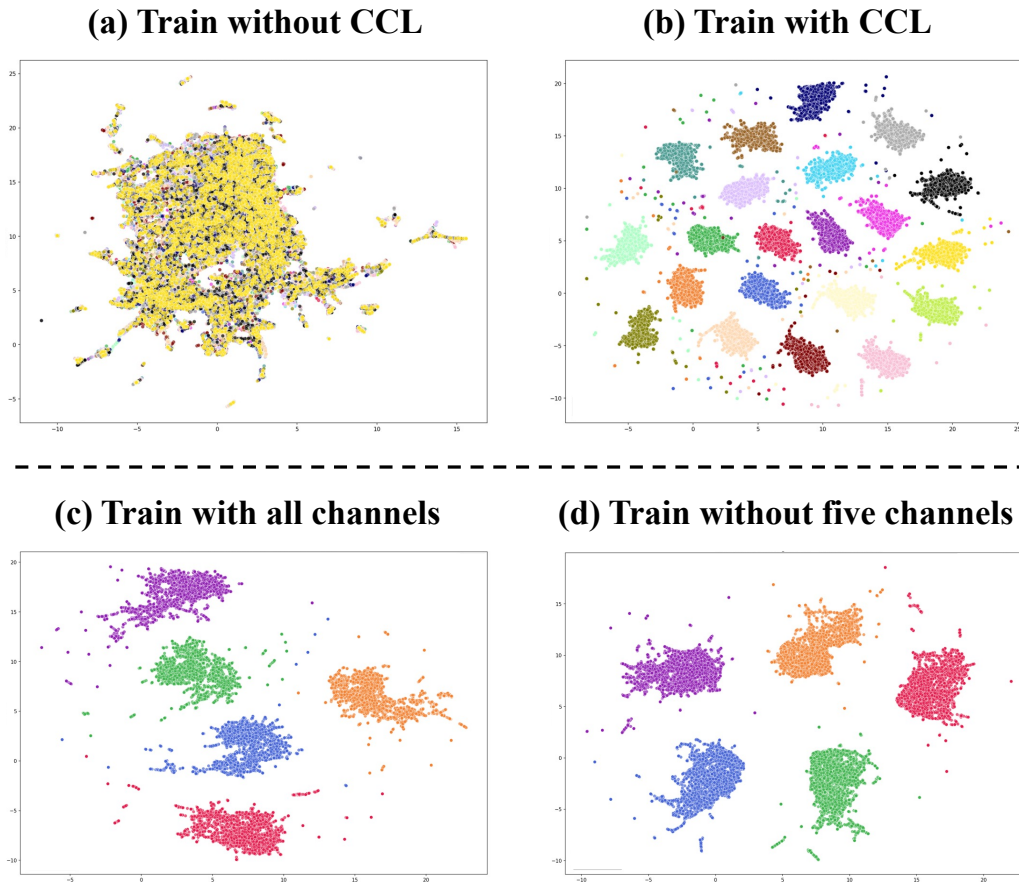


Figure 6: **Channel-wise EEG embedding visualizations on the TUAB dataset.** (a) Channel-wise EEG embeddings from the model trained without channel-level contrastive learning (CCL). (b) Channel-wise EEG embeddings from the model trained with CCL. (c) Channel-wise EEG embeddings for five channels (*i.e.*, F4, FZ, O1, P3, and T3) from the model trained using all channels. (d) Channel-wise EEG embeddings from the model trained excluding the five channels.

the embedding distributions of a fully-trained model (Figure 6(c)) with the channel-removed model (Figure 6(d)) reveals nearly identical clustering patterns. This indicates that our model intrinsically learns distinctive profiles for entirely unseen channels.

We further validate CCL’s adaptability on the CHB-MIT dataset, which employs a different montage. Consistent with previous results, Figure 7 shows that CCL is crucial for achieving clear channel separation, demonstrating its

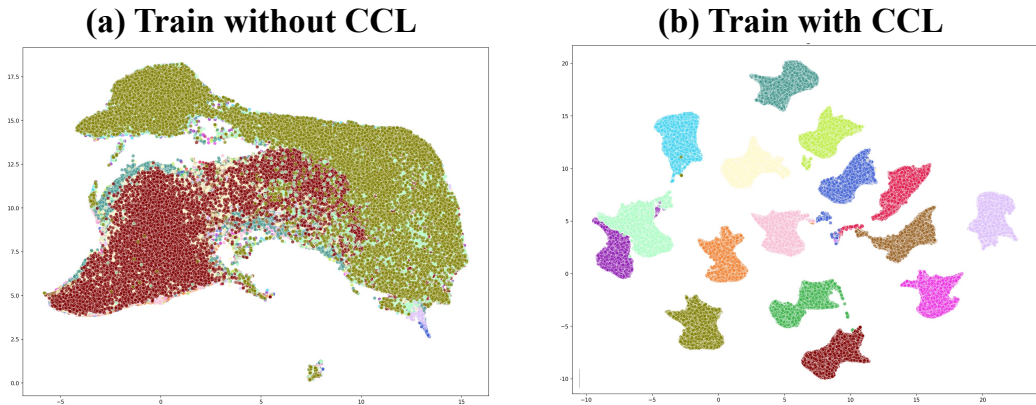


Figure 7: **Channel-wise EEG embedding visualizations on the CHB-MIT dataset.** (a) Channel-wise EEG embeddings from the model trained without channel-level contrastive learning (CCL). (b) Channel-wise EEG embeddings from the model trained with CCL.

broad applicability across datasets with significant channel heterogeneity.

Lastly, we demonstrate that representations for unseen channels are meaningfully derived from spatial relationships. By evaluating the model trained with masked channels, we computed cosine similarities for unseen channels F4 and FZ against the observed set (Figures 8(a) and 8(b)). Figure 8(a) shows that F4 exhibits the highest cosine similarity of 0.66 with its contralateral channel, F3, followed by a strong similarity with the adjacent channel C4. Similarly, Figure 8(b) indicates that FZ is most similar to CZ (0.59), its adjacent midline channel, while also showing high similarity with FP1. Consequently, the model effectively exploits learned spatial topologies to estimate accurate features for missing channels.

### 5.3. Finetuning classification performance

In Experiment 3, we investigate the cross-dataset generalization capabilities of the proposed framework. To achieve this, we append a classifier head to our pretrained EEG encoder and evaluate its transferability across multiple datasets. To rigorously assess generalization and resilience to channel variations, we primarily focus on the linear-probing setting, wherein the EEG encoder remains frozen and only the classifier is optimized. Additionally, to ensure an equitable comparison with prior baseline models, we also report outcomes under a full-finetuning paradigm.

First, we detail the linear-probing results on the TUAB dataset using EEG-CLIP as the baseline. As demonstrated in Table 6, our model consistently

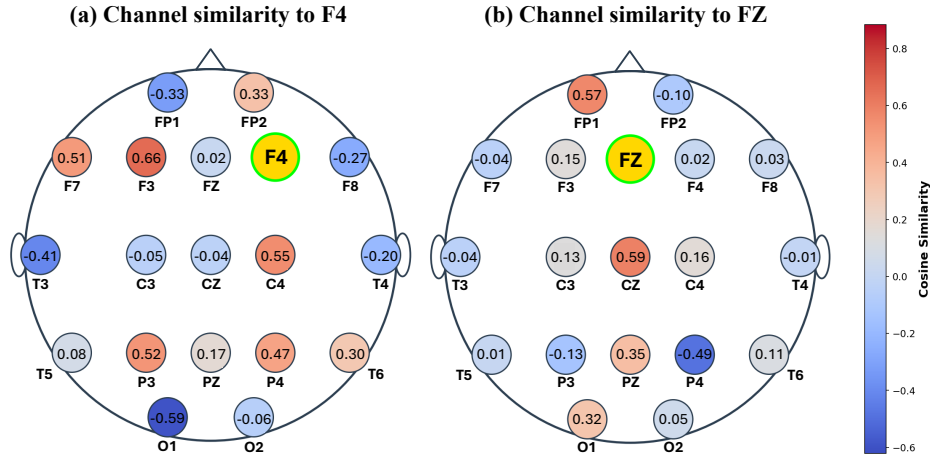


Figure 8: **Visualization of the mean cosine similarity between channel embeddings.** We evaluate the similarity for two channels (*i.e.*, F4 and FZ) using the model trained while excluding five channels (*i.e.*, F4, FZ, O1, P3, and T3). (a) Mean cosine similarity between the F4 embedding and the embeddings of other channels. (b) Mean cosine similarity between the FZ embedding and the embeddings of other channels.

Table 6: **TUAB dataset classification with a trained classifier head.** This table reports linear-probing performance on the three TUAB tasks.

Methods	<i>pathological</i>	<i>gender</i>	<i>age</i>
EEG-CLIP	$0.8148 \pm 0.0026$	$0.5798 \pm 0.0018$	$0.6840 \pm 0.0003$
<b>Proposed</b>	<b><math>0.8356 \pm 0.0011</math></b>	<b><math>0.6747 \pm 0.0020</math></b>	<b><math>0.7348 \pm 0.0024</math></b>

surpasses EEG-CLIP across all evaluated tasks, notably achieving an absolute improvement of over 9% in gender classification.

Second, we examine downstream generalization using the CHB-MIT and MUMTAZ datasets. As Table 7 illustrates, the proposed architecture establishes new state-of-the-art performance in both linear-probing and full-finetuning scenarios. During full-finetuning, our model outperforms LaBraM — currently the most competitive brain foundation model — by approximately 11.9% in balanced accuracy and over 5.3% in AUC-PR, a crucial metric for imbalanced data. Remarkably, even when restricted to linear-probing, our framework outperforms LaBraM by roughly 9.1% in balanced accuracy.

Finally, Table 8 highlights our model’s performance on the MUMTAZ dataset, where our linear-probing setup exceeds previous state-of-the-art

Table 7: **CHB-MIT dataset classification with a trained classifier head.** This table reports performance on seizure detection on the CHB-MIT dataset.

Methods	Balanced accuracy	AUC-PR
EEGNet	0.5658 $\pm$ 0.0106	0.1914 $\pm$ 0.0182
FFCL	0.6262 $\pm$ 0.0104	0.2049 $\pm$ 0.0346
BIOT	0.7068 $\pm$ 0.0457	0.3277 $\pm$ 0.0460
LaBraM-Base	0.7075 $\pm$ 0.0358	0.3287 $\pm$ 0.0402
EEG-CLIP	0.6843 $\pm$ 0.0601	0.2191 $\pm$ 0.0818
EEG-CLIP (LP)	0.5000 $\pm$ 0.0000	0.0981 $\pm$ 0.0233
<b>Proposed</b>	<b>0.8266 <math>\pm</math> 0.0506</b>	<b>0.3812 <math>\pm</math> 0.0648</b>
<b>Proposed (LP)</b>	<b>0.7988 <math>\pm</math> 0.0046</b>	<b>0.3689 <math>\pm</math> 0.0064</b>

Table 8: **MUMTAZ-2016 dataset classification.** This table reports performance on major depressive disorder classification on the MUMTAZ-2016 dataset, where LP denotes the linear-probing setting.

Methods	Balanced accuracy	AUC-PR
EEGNet	0.9232 $\pm$ 0.0104	0.9639 $\pm$ 0.0093
FFCL	0.9314 $\pm$ 0.0038	0.9717 $\pm$ 0.0021
BIOT	0.9358 $\pm$ 0.0052	0.9736 $\pm$ 0.0034
LaBraM-Base	0.9409 $\pm$ 0.0079	0.9798 $\pm$ 0.0093
EEG-CLIP	0.6582 $\pm$ 0.0095	0.6549 $\pm$ 0.0127
EEG-CLIP (LP)	0.5030 $\pm$ 0.0046	0.5548 $\pm$ 0.1032
<b>Proposed</b>	<b>0.9128 <math>\pm</math> 0.0084</b>	<b>0.9812 <math>\pm</math> 0.0043</b>
<b>Proposed (LP)</b>	<b>0.9439 <math>\pm</math> 0.0019</b>	<b>0.9900 <math>\pm</math> 0.0001</b>

benchmarks. Specifically, it surpasses unimodal baselines like BIOT and LaBraM, providing compelling evidence of robust cross-dataset adaptability. Interestingly, Table 8 also reveals that full-finetuning yields sub-optimal results compared to linear-probing on this dataset. We attribute this performance degradation to training set overfitting, a phenomenon consistent with catastrophic forgetting.

#### 5.4. Ablation study

The proposed method consists of three main components: channel attribute-based positional encoding (CAPE), dynamic channel projection (DCP), and dual-level contrastive learning (DCL). In Experiment 4, we conduct ablation

Table 9: **Ablation study on TUAB.** This table summarizes text-based classification performance on the TUAB dataset, where CAPE, DCP, and DCL denote channel attribute-based positional encoding, dynamic channel projection, and dual-level contrastive learning, respectively.

Methods	<i>pathological</i>	<i>gender</i>	<i>age</i>
w/o CAPE, DCP, DCL	0.7270	0.6633	0.4874
w/o DCP, DCL	0.7172	0.6545	0.4407
w/o DCL	0.8172	0.6300	0.6661
<b>Proposed</b>	<b>0.8158</b>	<b>0.6463</b>	<b>0.7125</b>

Table 10: **Ablation study on CHB-MIT.** This table summarizes text-based classification performance on the CHB-MIT dataset, where CAPE, DCP, and DCL denote channel attribute-based positional encoding, dynamic channel projection, and dual-level contrastive learning, respectively. All models are evaluated under the linear-probing setting.

Methods	Balanced accuracy	AUC-PR
w/o CAPE, DCP, DCL	0.7888 $\pm$ 0.0075	0.2970 $\pm$ 0.0059
w/o DCP, DCL	0.8002 $\pm$ 0.0071	0.2425 $\pm$ 0.0070
w/o DCL	0.7544 $\pm$ 0.0048	0.2576 $\pm$ 0.0064
<b>Proposed</b>	<b>0.7988 <math>\pm</math> 0.0046</b>	<b>0.3689 <math>\pm</math> 0.0064</b>

studies on TUAB, CHB-MIT, and MUMTAZ-2016 to validate the contribution of each component. The results for each dataset are reported in Table 9, Table 10, and Table 11, respectively.

As shown in Table 9, applying CAPE alone yields only limited gains. In contrast, combining CAPE with DCP leads to a substantial improvement, and the full model that includes all components achieves the best performance.

Table 10 shows that DCL achieves the largest performance gain on CHB-MIT. In contrast, applying CAPE alone reduces AUC-PR, indicating that the effect of a single component can be limited. Consistent with this, the full model achieves the highest AUC-PR, suggesting that the proposed components provide complementary benefits when used together. Moreover, because seizure detection on CHB-MIT is driven by correctly identifying the positive (*i.e.*, seizure) class, we focus on AUC-PR, which summarizes precision–recall performance for the positive class.

Table 11 also shows a consistent trend of improving performance as CAPE, DCP, and DCL are added progressively. The full model achieves the best results, with a balanced accuracy of 0.9439 and an AUC-PR of 0.9900. These

Table 11: **Ablation study on MUMTAZ-2016.** This table summarizes text-based classification performance on the MUMTAZ-2016 dataset, where CAPE, DCP, and DCL denote channel attribute-based positional encoding, dynamic channel projection, and dual-level contrastive learning, respectively. All models are evaluated under the linear-probing setting.

Methods	Balanced accuracy	AUC-PR
w/o CAPE, DCP, DCL	$0.8936 \pm 0.0006$	$0.9610 \pm 0.0003$
w/o DCP, DCL	$0.9161 \pm 0.0015$	$0.9807 \pm 0.0004$
w/o DCL	$0.9300 \pm 0.0009$	$0.9836 \pm 0.0003$
<b>Proposed</b>	<b><math>0.9439 \pm 0.0019</math></b>	<b><math>0.9900 \pm 0.0001</math></b>

results suggest that the proposed components contribute in a complementary manner.

### 5.5. EEG-text retrieval

In this experiment, we assess the cross-modal EEG-text retrieval capabilities of our proposed architecture. Motivated by a practical clinical scenario—where practitioners retrieve historical case reports based purely on novel EEG recordings to guide diagnostic decisions—we compute the cosine similarity between the retrieved text and the ground-truth clinical report for a given TUAB EEG query. Following the evaluation protocol of (Huang et al., 2021), we quantify retrieval efficacy using Precision@ $K$  ( $K \in \{1, 5, 10, 100\}$ ) across three core TUAB classification tasks: *pathology*, *gender*, and *age*.

As detailed in Table 12, precision is defined as the proportion of correctly labeled reports within the top- $K$  retrieved instances. Our CAMEL-CLIP model demonstrates consistent superiority over the baseline across all tasks. Notably, at  $K = 1$ , the proposed method yields absolute precision gains of 10.4% and 10.1% for the gender and age tasks, respectively. Figure 9 presents the actual results of the EEG-text retrieval task in the TUAB dataset conducted by CAMEL-CLIP. Figure 9 (a) illustrates the original report of the EEG sample used as a query, while Figure 9 (b) displays the training set reports retrieved by the model and ranked by similarity. A comparison between Figure 9 (a) and (b) reveals that key clinical terms such as "Right hemisphere focal slowing", "sharp waves", and "stroke" appear consistently in both. These results suggest that the proposed model captures patterns associated with neurological conditions as well as broader patient information encoded in EEG signals, and aligns them effectively with the text space. These

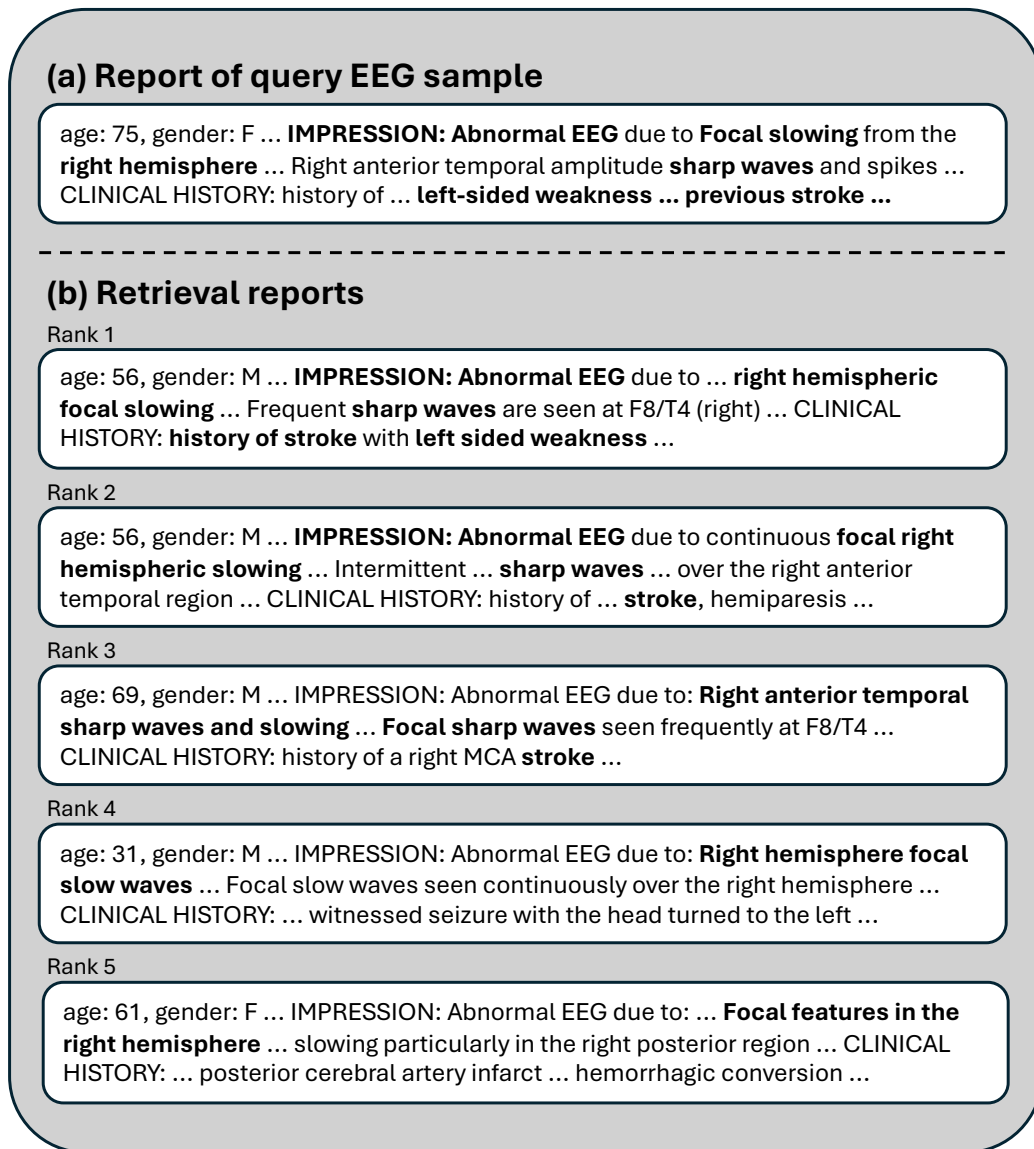


Figure 9: **Sample of EEG-text retrieval from the TUAB dataset.** (a) Text report of query EEG sample. (b) Retrieval report.

Table 12: **Precision on the retrieval task.** This table reports retrieval precision on the three TUAB tasks. Precision is computed as the fraction of retrieved reports within the top- $K$  results whose labels match the ground-truth label.

Methods	<i>pathological</i>	<i>gender</i>	<i>age</i>
EEG-CLIP @ 1	0.7994	0.5273	0.5924
EEG-CLIP @ 5	0.7752	0.5316	0.5875
EEG-CLIP @ 10	0.7733	0.5331	0.5899
EEG-CLIP @ 100	0.7731	0.5319	0.5940
<b>Proposed @ 1</b>	<b>0.8182</b>	<b>0.6316</b>	<b>0.6938</b>
Proposed @ 5	0.8136	0.6394	0.6712
Proposed @ 10	0.8132	0.6365	0.6631
Proposed @ 100	0.8129	0.6338	0.6555

results indicate that CAMEL-CLIP successfully extracts both neurological anomalies and broader demographic markers from raw EEG data, seamlessly mapping them into the textual domain. Consequently, the retrieved reports supply highly accurate clinical context—such as symptom profiles and expert interpretations—substantially enhancing their viability as decision-support tools in real-world medical environments.

## 6. Conclusion

We introduce CAMEL-CLIP, a multimodal EEG–text foundation model designed to maintain robustness under varying channel configurations. To explicitly address channel heterogeneity, CAMEL-CLIP incorporates three key components: (1) CAPE, which encodes channels based on semantic attributes rather than fixed positional indices; (2) DCP, which enables flexible handling of variable-length channel inputs; and (3) DCL, which jointly optimizes channel-wise and global feature representations.

By directly resolving the structural limitations imposed by heterogeneous channel configurations, CAMEL-CLIP establishes a strong foundation for building generalizable brain models. The proposed framework achieves substantially improved EEG–text alignment, yielding performance gains of up to 23.6% compared to existing multimodal methods. Through CCL, the EEG encoder captures fine-grained, channel-specific characteristics, allowing it to generate high-quality representations even for previously unseen channel layouts.

Extensive experiments demonstrate that CAMEL-CLIP effectively mitigates channel-induced domain shifts and achieves state-of-the-art performance across diverse downstream tasks. It outperforms the current state-of-the-art unimodal foundation model by 9.1% in balanced accuracy using only linear-probing. In addition, its enhanced cross-modal retrieval capability facilitates efficient identification of clinically relevant cases and associated reports, offering clinicians enriched contextual information to support more precise and reliable diagnostic decisions.

Despite these promising results, multimodal EEG–text modeling continues to face a fundamental challenge: the limited availability of large-scale, high-quality paired datasets that fully capture the complexity of EEG signals. Consequently, future work should more systematically investigate strategies to mitigate representation degradation under limited paired data. Potential directions include leveraging additional modalities to provide richer supervisory signals, developing EEG-specific augmentation schemes, and designing more principled pairing and alignment algorithms between EEG and text. Progress along these lines may further enhance the robustness and clinical applicability of multimodal EEG-text models.

## References

- Ay, B., Yildirim, O., Talo, M., Baloglu, U.B., Aydin, G., et al., 2019. Automated depression detection using deep representation and sequence learning with EEG signals. *J. Med. Syst.* 43, 205. <https://doi.org/10.1007/s10916-019-1345-y>.
- Chen, Z., Qin, C., You, W., Liu, R., Chu, C., et al., 2025. HEAR: An EEG foundation model with heterogeneous electrode adaptive representation. arXiv preprint arXiv:2510.12515.
- Devlin, J., Chang, M.W., Lee, K., Toutanova, K., 2019. BERT: pretraining of deep bidirectional transformers for language understanding. In: *Proceedings of the 2019 Conference of the North American Chapter of the Association for Computational Linguistics: Human Language Technologies, Volume 1 (Long and Short Papers)*, pp. 4171–4186.
- Goldberger, A.L., Amaral, L.A.N., Glass, L., Hausdorff, J.M., Ivanov, P.C., et al., 2000. PhysioBank, PhysioToolkit, and PhysioNet: components of a

- new research resource for complex physiologic signals. *Circulation* 101(23), e215–e220. <https://doi.org/10.1161/01.CIR.101.23.e215>.
- Guttag, J., 2010. CHB-MIT scalp EEG database [dataset]. PhysioNet. <https://doi.org/10.13026/C2K01R>.
- Huang, K., Altosaar, J., Ranganath, R., 2019. ClinicalBERT: modeling clinical notes and predicting hospital readmission. arXiv preprint arXiv:1904.05342.
- Huang, S.C., Shen, L., Lungren, M.P., Yeung, S., 2021. GLoRIA: A multimodal global-local representation learning framework for label-efficient medical image recognition. In: *Proceedings of the IEEE/CVF International Conference on Computer Vision (ICCV)*, pp. 3942–3951. <https://doi.org/10.1109/ICCV48922.2021.00391>.
- Jasper, H.H., 1958. The ten-twenty electrode system of the international federation. *Electroencephalogr. Clin. Neurophysiol.* 10, 371–375.
- Jiang, W.B., Zhao, L.M., Lu, B.L., 2024. Large brain model for learning generic representations with tremendous EEG data in BCI. In: *The Twelfth International Conference on Learning Representations (ICLR 2024)*.
- Kuruppu, G., Ramasubbu, D., Kaplan, D., Tang, S., Shanechi, M., Sani, O.G., 2025. EEG foundation models: a critical review of current progress and future directions. arXiv preprint arXiv:2507.11783.
- Lawhern, V.J., Solon, A.J., Waytowich, N.R., Gordon, S.M., Hung, C.P., Lance, B.J., 2018. EEGNet: a compact convolutional neural network for EEG-based brain–computer interfaces. *J. Neural Eng.* 15(5), 056013. <https://doi.org/10.1088/1741-2552/aace8c>.
- Li, H., Ding, M., Zhang, R., Xiu, C., 2022. Motor imagery EEG classification algorithm based on CNN-LSTM feature fusion network. *Biomed. Signal Process. Control* 72, 103342. <https://doi.org/10.1016/j.bspc.2021.103342>.
- McInnes, L., Healy, J., Melville, J., 2018. UMAP: Uniform manifold approximation and projection for dimension reduction. arXiv preprint arXiv:1802.03426.
- Mumtaz, W., 2016. MDD patients and healthy controls EEG data [dataset]. figshare. <https://doi.org/10.6084/m9.figshare.4244171.v2>.

- Ndir, T.C., Schirrmester, R.T., Ball, T., 2025. EEG-CLIP: learning EEG representations from natural language descriptions. *Front. Robot. AI* 12, 1625731. <https://doi.org/10.3389/frobt.2025.1625731>.
- Obeid, I., Picone, J., 2016. The Temple University Hospital EEG data corpus. *Front. Neurosci.* 10, 196. <https://doi.org/10.3389/fnins.2016.00196>.
- Patil, S., Schirrmester, R.T., Hutter, F., Ball, T., 2024. CoordConformer: heterogeneous EEG datasets decoding using transformers. In: *ICML 2024 Workshop on Geometry-grounded Representation Learning and Generative Modeling*.
- Radford, A., Kim, J.W., Hallacy, C., Ramesh, A., Goh, G., et al., 2021. Learning transferable visual models from natural language supervision. In: *Proceedings of the 38th International Conference on Machine Learning (ICML)*, PMLR 139, pp. 8748–8763.
- Saha, S., Baumert, M., 2020. Intra- and inter-subject variability in EEG-based sensorimotor brain computer interface: a review. *Front. Comput. Neurosci.* 13, 87. <https://doi.org/10.3389/fncom.2019.00087>.
- Shoeb, A.H., 2009. Application of machine learning to epileptic seizure onset detection and treatment. Ph.D. thesis, Massachusetts Institute of Technology.
- Shoeibi, A., Khodatars, M., Ghassemi, N., Jafari, M., Moridian, P., et al., 2021. Epileptic seizures detection using deep learning techniques: a review. *Int. J. Environ. Res. Public Health* 18, 5780. <https://doi.org/10.3390/ijerph18115780>.
- Solis-Escalante, T., Tapia-Gallardo, A., de la Hoz-Franco, E.Y., Gomez-Gil, P., Amezcua-Sanchez, J.P., 2024. Machine and deep learning trends in EEG-based detection and diagnosis of Alzheimer’s disease: a systematic review. *Eng. Proc.* 68(1), 78.
- Song, Y., Zheng, Q., Liu, B., Gao, X., 2023. EEG conformer: convolutional transformer for EEG decoding and visualization. *IEEE Trans. Neural Syst. Rehabil. Eng.* 31, 710–719. <https://doi.org/10.1109/TNSRE.2022.3230250>.
- van den Oord, A., Li, Y., Vinyals, O., 2018. Representation learning with contrastive predictive coding. *arXiv preprint arXiv:1807.03748*.

- Wang, J., Zhao, S., Li, S., Niu, H., Hou, B., Zhang, P., 2024. CBraMod: a criss-cross brain foundation model for EEG decoding. arXiv preprint arXiv:2412.07236.
- Xiong, W., Li, J., Li, J., Zhu, K., 2025. EEG-FM-Bench: a comprehensive benchmark for the systematic evaluation of EEG foundation models. arXiv preprint arXiv:2508.17742.
- Yan, R., Li, Y., Ding, H., Wang, F., 2025. Cross-domain EEG-based emotion recognition with contrastive learning. arXiv preprint arXiv:2511.05293.
- Yang, C., Westover, M.B., Sun, J., 2023. BIOT: Biosignal transformer for cross-data learning in the wild. In: Advances in Neural Information Processing Systems (NeurIPS) 36, pp. 78240–78260.
- Yao, D., Qin, Y., Hu, S., Dong, L., Vega, M.L.B., Sosa, P.A.V., 2019. Which reference should we use for EEG and ERP practice? *Brain Topogr.* 32(4), 530–549. <https://doi.org/10.1007/s10548-019-00707-x>.
- Yi, K., Wang, Y., Ren, K., Li, D., 2023. Learning topology-agnostic EEG representations with geometry-aware modeling. In: Advances in Neural Information Processing Systems (NeurIPS) 36, pp. 53875–53891.
- Zhang, W., Duan, Y., Lin, C.T., 2025. Brain foundation models: a survey on advancements in neural signal processing and brain discovery. arXiv preprint arXiv:2503.00580.